Applied Radiation and Isotopes 170 (2021) 109599

Contents lists available at ScienceDirect

Applied Radiation and Isotopes

journal homepage: http://www.elsevier.com/locate/apradiso

Impact of prompt gamma emission of ^{44}Sc on quantification in preclinical and clinical PET systems

Florian Rosar [a,b,*], Hendrik Bohnenberger [a], Euy Sung Moon [c], Frank Rösch [c], Achim Denig [d], Daniel Vincenz-Zörner [e], Manuela A. Hoffmann [b], Fadi Khreish [a], Samer Ezziddin [a], Mathias Schreckenberger [b], Hans-Georg Buchholz [b,1], Andrea Schaefer-Schuler [a,1]

[a] Dep. of Nuclear Medicine, Saarland University, Homburg, Germany
[b] Dep. of Nuclear Medicine, University of Mainz, Mainz, Germany
[c] Dep. of Chemistry – TRIGA Site, University of Mainz, Mainz, Germany
[d] Dep. of Nuclear Physics, University of Mainz, Mainz, Germany
[e] Mediso GmbH – Medical Imaging Systems, Münster, Germany

ARTICLE INFO

Keywords:
Scandium-44
PET
Quantification
Prompt gamma
Correction

ABSTRACT

^{44}Sc is an increasingly investigated positron emitter for use in positron emission tomography (PET) imaging. However, ^{44}Sc is a non-pure positron emitter, since prompt photons are co-emitted during the decay process. This study investigates coincidence energy spectra of ^{44}Sc and its impact on PET quantification on a preclinical and clinical PET system in comparison with ^{18}F. The raw data of the coincidence events revealed characteristic differences comparing the photon energy distribution of ^{44}Sc and ^{18}F. Due to prompt gamma emission of ^{44}Sc, activity recovery is underestimated on PET systems. However, clinical PET imaging of ^{44}Sc with acceptable quantitative accuracy appears feasible by using a single, constant correction factor.

1. Background

In the last decade, the radionuclide scandium-44 (^{44}Sc) has gained increasing attention in medical research and radiopharmaceutical development for use in positron emission tomography (PET) imaging (Müller et al., 2018). The development of a ^{44}Ti/^{44}Sc generator system (Filosofov et al., 2010; Roesch, 2012) and the possibility to produce ^{44}Sc with a cyclotron using calcium targets (Severin et al., 2012; Krajewski et al., 2013; van der Meulen et al., 2015) are poised to ensure the availability of the radionuclide. In addition to the possibility of decentralized production with distribution to outsourced PET centers, a half-life of about 4 h opens up the possibility of observing biological processes that are subject to slow kinetics and require acquisitions up to 24 h p.i. (Umbricht et al., 2017; Müller et al., 2018). Recent phantom studies revealed superior image resolution of ^{44}Sc compared to the widely used ^{68}Ga in preclinical setting (Bunka et al., 2016; Rosar et al., 2020). Due to the chemical similarity of the $^{44}Sc^{3+}$ to the $^{68}Ga^{3+}$, stable complexes can be formed with already clinically established chelators such as DOTA (1,4,7,10-tetraazacyclododecane-1,4,7,10-tetraacetic acid) (Huclier-Markai et al., 2011; Majkowska-Pilip and Bilewicz, 2011; Pruszyński et al., 2012; Domnanich et al., 2016). In recent years, several preclinical studies on ^{44}Sc-labelled tracers have been performed, which have shown promising results (Koumarianou et al., 2012; Eigner et al., 2013; Honarvar et al., 2017; Nagy et al., 2017). First clinical studies with [^{44}Sc]Sc-PSMA-617 and [^{44}Sc]Sc-DOTA-TOC confirmed the potential benefit of using ^{44}Sc in PET in humans (Eppard et al., 2017; Singh et al., 2017; Khawar et al., 2018).

^{44}Sc decays by positron emission with a branching fraction of 94.3% and by electron capture with about 5.7%. However, ^{44}Sc is a non-pure positron emitter, since prompt photons are co-emitted during the decay process to stable ^{44}Ca. Fig. 1 presents the decay scheme of ^{44}Sc. Although these prompt photons have an energy (mainly 1157 keV) above the conventional PET detection energy range, they can influence PET data acquisition after scattering with matter and associated loss in energy. As known for other non-pure positron emitters (e.g. ^{86}Y and ^{124}I), additionally emitted photons can lead to random as well as multiple coincidences. This can result in a different energy distribution of the coincidently detected photon pairs, which may in turn lead to an

* Corresponding author. Department of Nuclear Medicine Saarland University Kirrberger, Str. 100, Geb. 50, D-66421, Homburg, Germany.
E-mail address: florian.rosar@uks.eu (F. Rosar).
[1] Shared senior authorship.

https://doi.org/10.1016/j.apradiso.2021.109599
Received 23 September 2020; Received in revised form 21 December 2020; Accepted 14 January 2021
Available online 21 January 2021

incorrectly calculated activity in the reconstructed images, as PET systems are calibrated based on a normalization to the pure-positron emitter ^{18}F.

There is only one study, recently published by Lima et al. (2020) focusing on quantification of ^{44}Sc in PET. These authors state that further work on corrections is still necessary to improve the quantitative accuracy of ^{44}Sc in PET. In this context investigation of coincidence energy spectra of ^{44}Sc and its influence on PET quantification is of high importance but has not been published so far. In an attempt to close this gap, we performed phantom measurements on a preclinical and a clinical PET system. We analyzed the energy distribution in raw data and the recovered activity in the reconstructed images and compared it with ^{18}F, the most common used pure positron emitter in nuclear medicine.

2. Material and methods

2.1. Radionuclides

2.1.1. ^{44}Sc

^{44}Sc was obtained from a ^{44}Ti/^{44}Sc generator system that was developed at the Institute of Nuclear Chemistry at Mainz University, Germany (Filosofov et al., 2010). Briefly, ~170 MBq of ^{44}Sc were eluted with 20 ml of a mixture consisting of 0.07 M hydrochloric acid and 0.005 M oxalic acid. ^{44}Sc was trapped on a cation exchange resin (AG 50W-X8) and eluted with 3 ml of a 0.25 M ammonium acetate solution (pH4). This procedure resulted in ~130 MBq of ^{44}Sc containing less than 10 Bq of ^{44}Ti-activity (Roesch, 2012). Quality control included thin-layer chromatography (TLC) for chemical purity and gamma-spectroscopy for radionuclidic purity (Pruszyński et al., 2010). The activity of ^{44}Sc was measured in a dose calibrator (Nuvia ISOMED, 2010; Nuvia Instruments, Dresden, Germany) using ^{18}F-calibration settings. A conversion factor of 0.70 to account for absolute ^{44}Sc activity was applied, which was initially evaluated by the group of Roesch in comparison to spectrometry measurements on a calibrated Ge(Li) detector (Roesch, 2012).

2.1.2. ^{18}F

^{18}F was used as commercially purchased ^{18}F-fluorodeoxyglucose (Life Radiopharam f-con GmbH, Holzhausen, Germany). The activity of the samples used was determined in a dose calibrator (Nuvia ISOMED, 2010; Nuvia Instruments, Dresden, Germany).

2.2. PET systems and reconstructions

2.2.1. Mediso nanoScan PET/MRI

The nanoScan PET/MRI (Mediso Medical Imaging Systems, Budapest, Hungary), in the following referred to as “nanoScan”, is a hybrid small animal scanner consisting of a 12-detector block PET system and a 1-T magnet resonance imaging (MRI) system. Every detector block is composed of 39 × 81 lutetium-yttrium oxyorthosilicate (LYSO) crystals with dimensions of 1.12 mm × 1.12 mm x 13.00 mm (total crystal number: 37908). The effective axial field of view (FOV) spans 94 mm. According to the manufacturer, the PET spatial resolution is 700 μm. The coincidence time window on the nanoScan is 5 ns.

2.2.2. Siemens Biograph 40 mCT PET/CT

The Siemens Biograph 40 mCT (Siemens Medical Solutions, Knoxville, USA), in the following referred to as “Biograph”, is a clinically established human hybrid PET/CT scanner. The PET system consists of a total of 4 rings, each with 48 detector blocks, which are each constructed from a 13 × 13 grid of 4 mm × 4 mm x 20 mm lutetium oxyorthosilicate (LSO) crystals (total crystal number: 32448). The effective axial FOV is 216 mm. The coincidence time window on the Biograph is 4.1 ns.

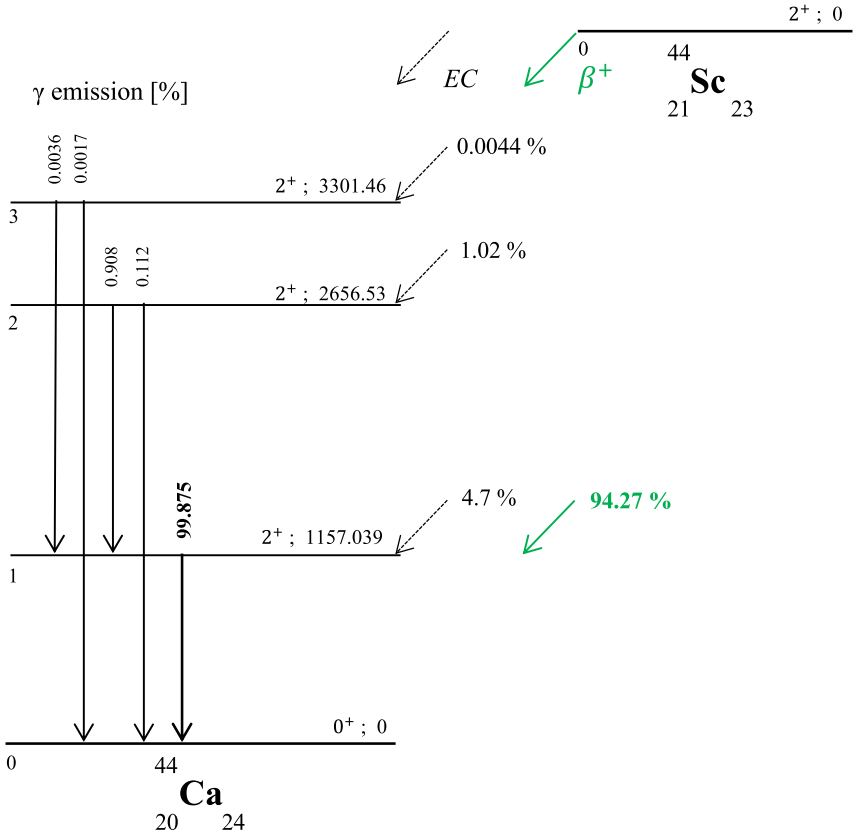

Fig. 1. Decay scheme of ^{44}Sc.

3. Reconstructions

Iterative TeraTomo-3D reconstruction based on an 3D ordered subset expectation maximization (OSEM) algorithm was performed on the nanoScan using the presets as recommended by the manufacturer (12 iterations, 6 subsets, normal regularization ($\alpha = 0.0005$), voxel size 0.4 mm × 0.4 mm x 0.4 mm, energy window used for reconstruction: 400–600 keV). On the Biograph, reconstruction settings were used that were previously validated within the EANM accreditation program EARL (Boellaard et al., 2015). These are: an iterative 3D-OSEM reconstruction with 3 iterations, 24 subsets, 5 mm Gaussian filtering, a voxel size of 4 mm × 4 mm x 5 mm and an energy window used for reconstruction of 435–650 keV). As recommend by EARL, no additional time-of-flight (TOF) or point-spread function (PSF) modelling techniques were applied. In the context of our study, these reconstruction settings are termed standard reconstruction settings. To convert the measured coincidences into activity values, a normalization was used, which was created during the calibration of the respective scanner for ^{18}F. On both scanners the specific half-lives and branching fractions of ^{44}Sc and ^{18}F were taken into account in the reconstruction process. All reconstructions included corrections for scatter, attenuation, dead time and decay as implemented by the respective manufacturer. On the nanoScan, scatter and attenuation correction are performed based on an MRI-based material map, whereas on the Biograph these corrections are based on a low-dose CT.

3.1. Phantoms

In the preclinical setting on the nanoScan, the well-known standardized image quality phantom NEMA NU 4–2008 (National Electrical Manufacturers Associaton (NEMA), 2008) was used (capacity 30 ml), in the clinical setting on the Biograph, a cylindrical PMMA (polymethylmethacrylate) phantom (inner/outer length: 240/300 mm, inner/outer diameter: 175/195 mm, capacity 6 l). Both phantoms were filled with various activities of ^{44}Sc and ^{18}F, respectively.

4. Measurements and analysis

4.1. Energy spectra of coincidence events

For the analysis of the energy spectra of coincidence events, measurements of the image quality phantom were performed on the nanoScan using a PET acquisition time of 60 s and activities for both nuclides (^{44}Sc, ^{18}F) ranging from 8 MBq down to 1 MBq. All measurements were repeated three times. The acquired listmode data, containing information of the energy of coincidence events, were exported and read out with an in-house MATLAB script (version 9.0, MathWorks, Natick, USA). Each event was analyzed with respect to the energy distribution. Hereby, a constant number of events (the first $n = 10^6$ events) was taken into account. Furthermore, the coincidence rates and the pile-up factors, used for dead time correction, were exported and compared.

4.2. Activity recovery

Analysis of activity recovery was done on both scanners with ^{44}Sc and ^{18}F. Successive PET scans with both radionuclides were acquired for 30 min each with activities ranging from 8 to 1 MBq on the nanoScan and 80 to 10 MBq on the Biograph. All measurements were repeated three times. The reconstructed PET data were analyzed with the software packages PMOD (version 4.1, PMOD Technologies LLC, Zurich, Switzerland) and Rover (version 2.1.1.12, ABX advanced biochemical compounds GmbH, Radeberg, Germany). Mean reconstructed activity concentration was determined using a cylindrical 'Volume-of-Interest' (VOI) of approximately 5 ml in the Image quality phantom and of approximately 3500 ml in the cylindrical phantom, each placed in the middle part of the main chamber of the respective phantom. The entire reconstructed activity in the phantom was extrapolated by multiplying the mean activity concentration in the VOI with the corresponding phantom volume.

5. Results

5.1. Energy spectra of coincidence events

The raw data of the coincidence events (detection range: 0–1022 keV) read out on the nanoScan revealed characteristic differences comparing the photon energy distribution of ^{44}Sc and ^{18}F.

With ^{44}Sc compared to ^{18}F, a higher number of detected photons was measured in the range of 150–400 keV ("Compton peak") and in the peripheral regions (<150 keV, > 750 keV), whereas a smaller number was found in the ranges of 400–600 keV ("511 keV photopeak") and 600–750 keV. Fig. 2 exemplifies the resulting energy spectra for both ^{44}Sc and ^{18}F, which were measured for a number of $n = 10^6$ coincidence

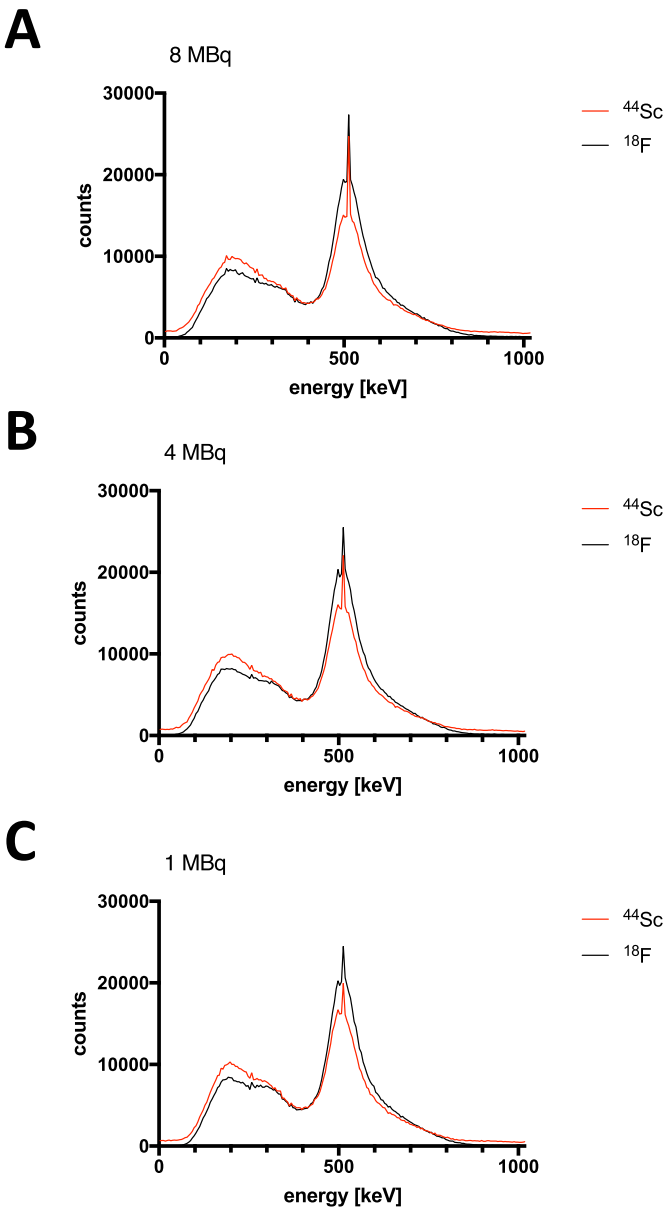

Fig. 2. Energy spectra of ^{44}Sc (red) and ^{18}F (black) using 8 MBq [A], 4 MBq [B] and 1 MBq [C]. (For interpretation of the references to colour in this figure legend, the reader is referred to the Web version of this article.)
(Histograms shown with bin of 5 keV).

events and phantom activities of 8, 4 and 1 MBq. A table summarizing the average percentage energy distribution of the detected photons depending on the activity used is presented in the supplement material (Table S1). Comparing the results for the different applied phantom activities, only small variations were observed.

In addition, these features are pointed up in Fig. 3 showing the energy distribution pattern of the two photons of coincidently detected photon pairs. For illustrative purposes, samples of $n = 10^4$ coincidence events were plotted. On the nanoScan, only those coincidence events with energies of both coincidently detected photons between 400 and 600 keV were used for image reconstruction. The percentage of the measured events in this energy range averaged 17.2% (16.2–17.8%) for ^{44}Sc and 24.4% (23.2–25.0%) for ^{18}F, corresponding to ratio of 0.706 (^{44}Sc/^{18}F) or a relative difference of −29.4%.

Fig. 4 shows the percentage of detected photon pairs in the energy range 400–600 keV depending on the activity used. A complete distribution of the photon pairs is given in the supplement material (Table S2).

The analysis of the coincidence rate over the entire energy spectra and the pile up factors revealed a higher coincidence rate for ^{44}Sc than for ^{18}F (mean difference +9.3%) (Fig. 5a), while similar pile up factors were observed for both radionuclides (mean difference of 0.5%) (Fig. 5b).

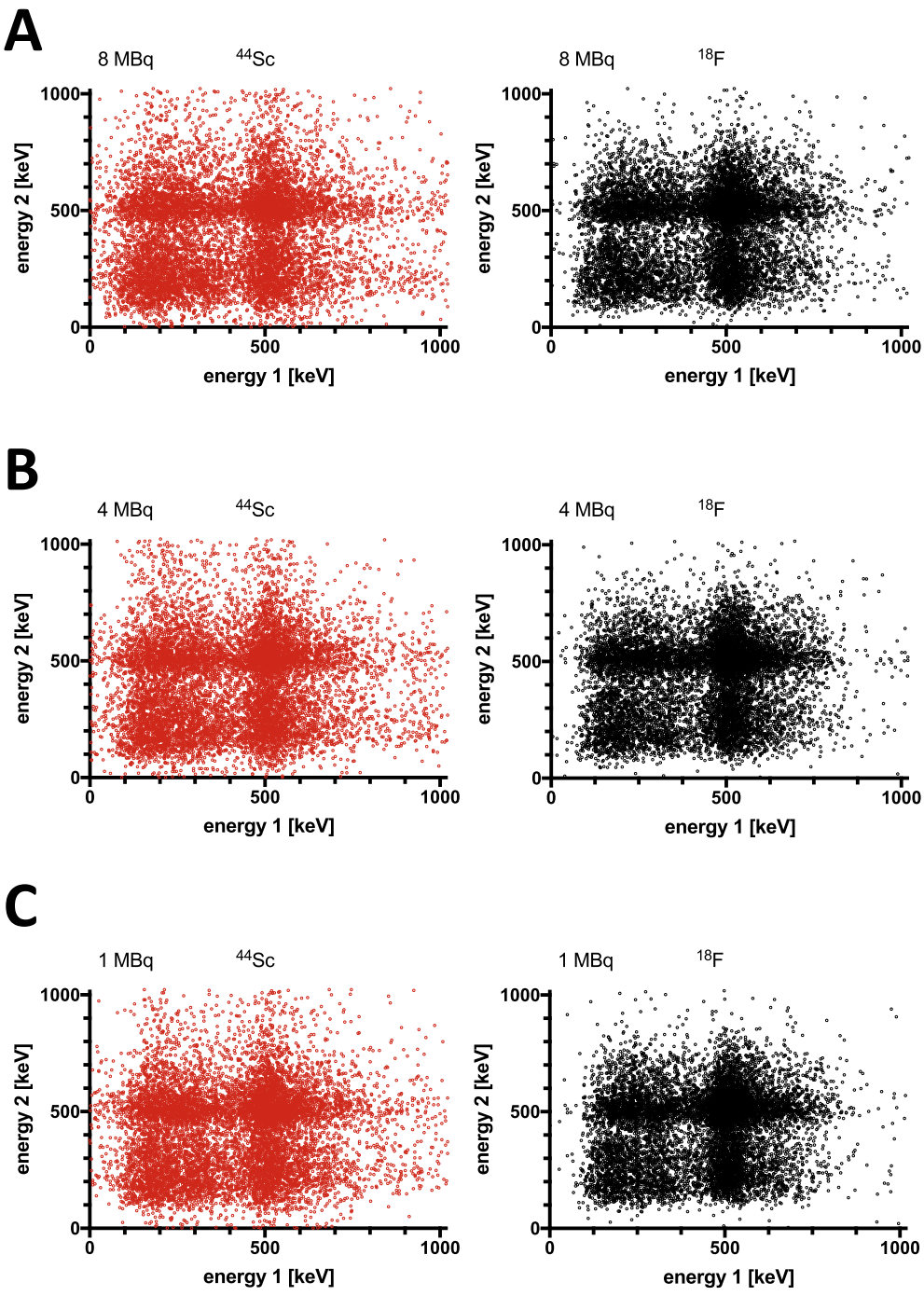

Fig. 3. Energy distribution pattern of the two photons of coincidently detected photon pairs for a sample of the first $n = 10^4$ coincidence events of ^{44}Sc (red) and ^{18}F (black) using 8 MBq [A], 4 MBq [B] and 1 MBq [C]. (For interpretation of the references to colour in this figure legend, the reader is referred to the Web version of this article.)

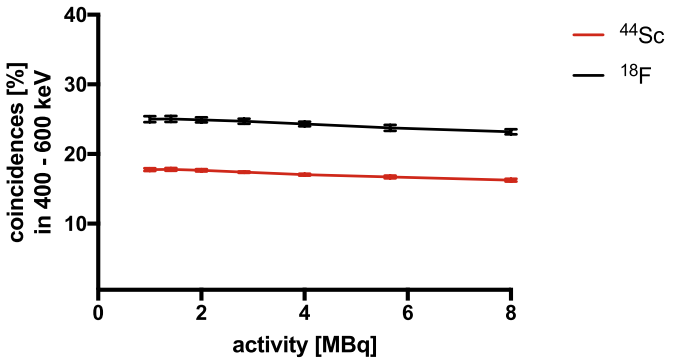

Fig. 4. Percentage of coincidently detected photon pairs in the energy range 400–600 keV for ^{44}Sc (red) and ^{18}F (black) depending on the activity used. (For interpretation of the references to colour in this figure legend, the reader is referred to the Web version of this article.)

5.2. Activity recovery

Compared to ^{18}F, the reconstructed image data sets revealed significantly lower values of reconstructed activity for ^{44}Sc on the nanoScan as well as on the Biograph. Notably, for both, ^{44}Sc and ^{18}F, a linear relationship between the true and reconstructed activity was found (Fig. 6). The corresponding linear regression analyses resulted in reconstructed PET activity of 73.5% (^{44}Sc) and 99.2% (^{18}F) for the nanoScan and of 78% (^{44}Sc) and 102.2% (^{18}F) for the Biograph.

Thus, compared to ^{18}F, the reconstructed activity for ^{44}Sc was lower by 26.0% on the nanoScan and by 27.3% on the Biograph. Consequently, to quantify ^{44}Sc PET measurements performed on a scanner with ^{18}F normalization, an inverse correction factor, 1.35 for the nanoScan and 1.31 for the Biograph, has to be considered.

6. Discussion

In the present study, phantom measurements with the non-pure positron emitter ^{44}Sc were performed to investigate the impact of prompt gamma emission on the accuracy of quantitative PET results.

The energy distribution of coincidently detected photon pairs of ^{44}Sc were compared to those of ^{18}F on a small animal PET/MRI (nanoScan). Furthermore, the activity recovery of both radionuclides in reconstructed images was determined for this small animal PET/MRI, and in addition, for a human PET/CT (Biograph). Results on both scanner types were compared. We used the corrections and the reconstruction parameters as recommended by the manufacturers and validated by the accreditation program, respectively.

In contrast to ^{18}F, ^{44}Sc is a non-pure positron emitter. In the decay process from ^{44}Sc to ^{44}Ca, additional prompt photons, so-called cascade photons, are emitted during decay. 99.9% of these photons have an energy of 1157 keV when they are generated, which is higher than the detection range normally used in PET (0–1022 keV). However, due to interaction with matter (primarily Compton scattering) those photons lose some of their energy. As a consequence, the detection of random cascade coincidences (coincidence of an annihilation photon and a cascade photon or of two cascade photons) or of triple coincidences (coincidence of two annihilation photons and a cascade photon) can occur. Therefore, differences in the respective energy spectra of coincidently detected photon pairs from ^{44}Sc and ^{18}F were expected and verified in the present study.

Considering the total of coincidently detected photons and

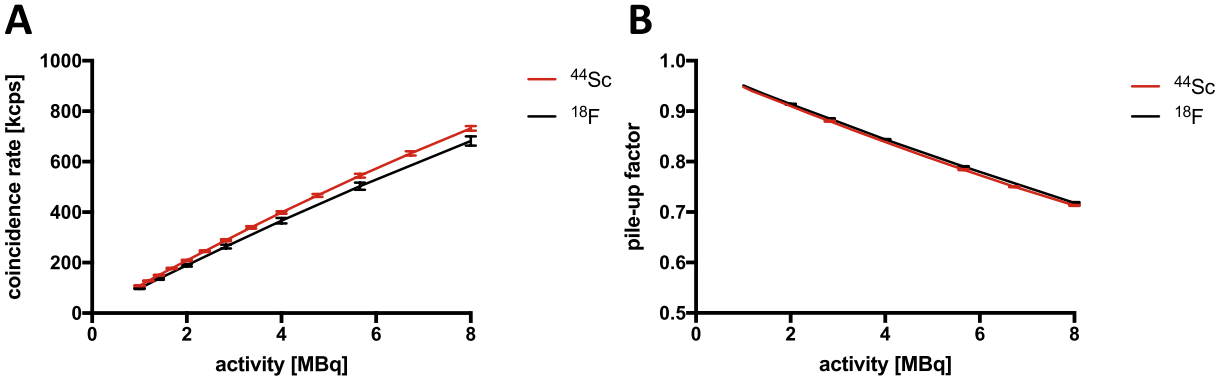

Fig. 5. Total coincidence rates [A] and pile-up factors [B] for ^{44}Sc (red) and ^{18}F (black) depending on the activity used. (For interpretation of the references to colour in this figure legend, the reader is referred to the Web version of this article.)

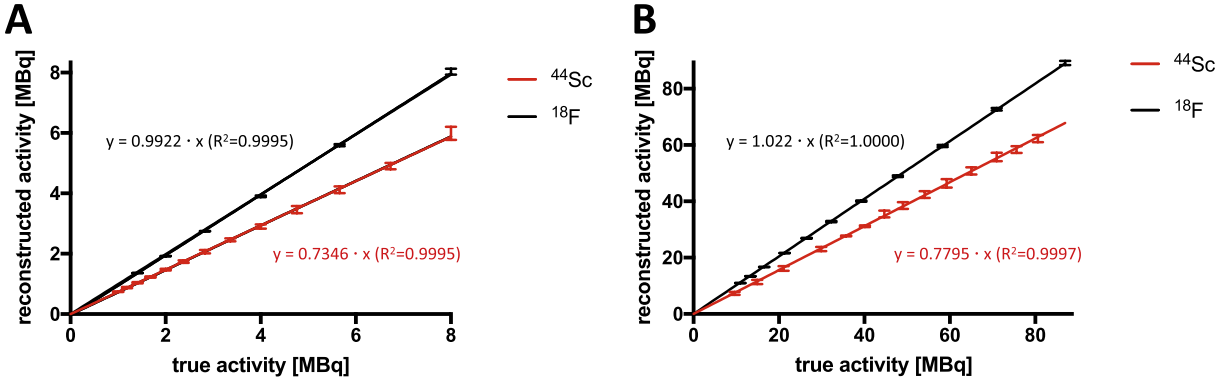

Fig. 6. Activity recovery for ^{44}Sc (red) and ^{18}F (black) on nanoScan [A] and Biograph [B]. (For interpretation of the references to colour in this figure legend, the reader is referred to the Web version of this article.)

comparing the results of ^{44}Sc and ^{18}F, a lower percentage of non-scattered annihilation photons was observed for ^{44}Sc in the energy ranges of 400–600 keV and 600–750 keV. In addition, a higher percentage was found in the energy ranges of 150–400 keV, < 150 keV and 750–1022 keV (see Figs. 2 and 3 and supplement material). As Compton scattering is the most prominent interaction for the ^{44}Sc gamma rays (energy 1157 keV), the detection of different cascade coincidence events could be expected resulting in the observed higher proportion of events in the energy ranges 150–400 keV, < 150 keV and 750–1022 keV in comparison to ^{18}F. However, triple coincidences also arise with only the first two of the three photons being stored on the nanoScan according to the manufacturer's specifications. The lower proportion of coincidence events in the range of the non-scattered annihilation photons (400–600 keV) for ^{44}Sc, compared to ^{18}F, may therefore be explained by loss of annihilation photons during data acquisition.

To ensure optimized PET image resolution, only those coincidence events are used for image reconstruction, when both photons are detected within a preselected energy window. On the nanoScan, this energy window is fixed to an energy range from 400 to 600 keV. Only about 17.2% and 24.4% of the coincidently detected photon pairs for ^{44}Sc and ^{18}F fulfilled this condition (see Fig. 4). The resulting significant difference between ^{44}Sc and ^{18}F of 7.2% absolute and 29.4% in percentage terms, respectively, should be explained, as mentioned above, by the impact of the contribution of the different cascade coincidences of ^{44}Sc. For all other coincidences, the energy requirement was not met for at least one of the two photons. Altogether, these results clearly show that PET detection includes a total of true, scattered and random coincidences.

Due to the additional cascade coincidences the coincidence rate for ^{44}Sc was, on average, only +9.3% higher than that for ^{18}F (see Fig. 5a) and showed only a very small influence on the dead time in the activity range considered in this study (deviation of the pile-up factors on average 0.5%, see Fig. 5b). In advance, we did expect larger differences in the coincidence rates between ^{44}Sc and ^{18}F. However, the small difference could be explained by the distinct lower interaction probability of high energy photons in the PET detector material.

To the best of our knowledge, similar studies on the analysis of coincidence spectra have not been published so far for ^{44}Sc, but for other non-pure positron-emitting PET nuclides such as ^{124}I and ^{76}Br (Cal-González et al., 2015). That publication reported differences in the coincidence spectra of the two radionuclides - similar to what was observed in our study for ^{44}Sc (a relative decrease of the coincidence events in the range 400–600 keV and increase in the range < 400 keV) (Cal-González et al., 2015). However, comparing the relative changes in the spectra of these two radionuclides and of ^{44}Sc, differences are observed which should be explained by the characteristic physical properties of the radionuclides. Here, the branching ratio and energy of prompt gamma quanta (positron emissions: 22.9% (^{124}I), 55.1% (^{76}Br), and 94.3% (^{44}Sc), major cascade photons 603 keV/62.9% (^{124}I), 559 keV/74.0% (^{76}Br), and 1157 keV/99.9% (^{44}Sc)) are of particular importance. Occurrence of random-, cascade- and triple-coincidences with varying frequencies could therefore be expected.

Activity recovery of ^{44}Sc and ^{18}F was significantly different in the reconstructed images on both, the small animal PET/MRI and the human PET/CT scanner. ^{18}F activity recovery was 99.2% on the nanoScan and 102.2% on the Biograph, respectively. Both values for ^{18}F are in accordance with the international quality guidelines in PET (Boellaard et al., 2015; Kaalep et al., 2018, 2019). Measurements of ^{18}F activity recovery on the clinical scanner are performed in our department quarterly. The results are approved by the EANM accreditation program EARL to reduce potential variabilities of quantification. In quantitative PET evaluations we solely apply the reconstruction parameters validated by EARL. In order to assure consistent image quality on the nanoScan as well, respective measurements for ^{18}F are also performed quarterly, using parameters proposed by the manufacturer. Our results confirm that the corrections as well as the normalization implemented for ^{18}F on the respective PET system were effective and valid. With ^{44}Sc, lower values of activity recovery (73.5% on nanoScan and 78.0% on Biograph) were observed. This resulted in a 26.0% (nanoScan) and 23.7% (Biograph) lower activity recovery for ^{44}Sc when compared to ^{18}F. Consequently, these results indicate that a reconstruction algorithm with parameters adapted to ^{18}F cannot simply be applied to ^{44}Sc by solely changing the nuclide-specific half-life and the branching fraction. This is in line with results of Lima et al. (2020), who performed recovery measurements for ^{44}Sc on the same human PET/CT scanner using one single activity. These authors calculated activity recoveries in the homogenous background region of 78% and 81%, depending on the scatter correction used, but independent on the number iterations (Lima et al., 2020).

For both, ^{18}F and ^{44}Sc, a strong correlation between reconstructed and true activity was observed on both PET systems (Fig. 6) but each is characterized by its own slope. Thus, this relative difference is independent of the activity used. Altogether, the activity recovery measurements revealed that, when compared to ^{18}F, the reconstructed activity of ^{44}Sc is systematically underestimated despite its slightly increased total coincidence rate (9.3% on nanoScan) and similar pile-up factors of both radionuclides. This may be due to the percentage of coincidence events being significantly smaller for ^{44}Sc as compared to ^{18}F in the energy range used for reconstruction (nanoScan: 400–600 keV, Biograph: 435–650 keV). Furthermore, the standard scatter correction may also be non-appropriate due to prompt gamma emission leading to an over-correction of scatter resulting in lower reconstructed activity (Lima et al., 2020).

Underestimation of activity in reconstructed images has also been observed for other non-pure PET nuclides such as ^{55}Co, ^{124}I, and ^{86}Y (Kull et al., 2004; Braad et al., 2015). Measurement on a comparable human PET/CT (GE Discovery PET/CT 690) showed deficient activity recoveries of 74.9% for ^{55}Co (positron emission 75.8%, major cascade photons 931 keV/75.0%) and of 73.0% for ^{124}I (Braad et al., 2015).

The linear relationship between true and reconstructed activities observed for both, ^{44}Sc and ^{18}F, allows the application of a constant correction factor to subsequently correct reconstructed ^{44}Sc activities measured on an ^{18}F calibrated PET scanner. Using the respective standard reconstruction settings, a correction factor of 1.35 was calculated for nanoScan, and of 1.31 for the Biograph. The difference between both values is due to the different detector geometry and different reconstruction settings of the two PET systems. In this context, it needs to be pointed out that the two values of the correction factor presented here are only valid for the respective scanner in combination with the applied reconstruction settings. Nevertheless, modification of one single component of the system, e.g. variation of the post-reconstruction filtering or variation of the scatter correction method, can change the measurement result for the calibration factor. Consequently, before ^{44}Sc is applied in vivo, it is mandatory that the correction factor needs to be determined by phantom measurements for each applied combination of PET scanner and reconstruction setting.

Uncorrected reconstructed ^{44}Sc activity, or activity concentration, can have significant impact on the quantitative results of preclinical and human studies. Calculated binding properties to target structures of newly developed ^{44}Sc tracers could be underestimated, thus falsely implying lower binding. Additionally, organ doses based on uncorrected quantification of ^{44}Sc PET could also be underestimated. The correction of reconstructed ^{44}Sc activities obtained with PET settings validated for ^{18}F, is therefore mandatory.

The correction of activity concentrations by a constant factor is easy to implement and should be applied. However, it must be thoroughly tested in (pre)clinical conditions in further studies in order to confirm its robustness. In addition, it has to be noted that this correction factor does not take into account possible background noise due to random cascade and triple coincidence, which was observed in previous studies for ^{44}Sc (Rosar et al., 2020) and other non-pure PET nuclides (Buchholz et al., 2003; Herzog et al., 2008; Lubberink and Herzog, 2011; Rösch et al.,

2017). More complex correction algorithms are necessary to address this. In the last decade, several different approaches, referred to as 'prompt gamma corrections' (PGC), have been published for other non-pure PET nuclides, ranging from analytical methods to Monte Carlo simulations (Conti and Eriksson, 2016). Recently, Lima et al. tested a model of PGC for ^{44}Sc and reached improvement of activity recovery to 87% (Lima et al., 2020). In future studies, PGC approaches should be further analyzed, improved and optimized for ^{44}Sc.

Besides ^{44}Sc, the isotope ^{43}Sc is also a promising radionuclide for PET imaging (positron emission: 88%, $E_{mean} = 0.48$ MeV, half-life = 3.89 h), albeit with less and lower concurrent emitted gamma rays (372.8 keV, 23%) (Domnanich et al., 2017; Walczak et al., 2015). Using ^{43}Sc instead of ^{44}Sc would likely allow for a more adequate quantification in PET. However, the availability of ^{43}Sc is limited due to the absence of a radionuclide generator system. The production of ^{43}Sc requires a particle accelerator, is challenging and cost extensive (Huclier-Markai et al., 2018; Mikolajczak et al., 2019). This might contribute to the fact that there are fewer studies using ^{43}Sc than ^{44}Sc, despite its known advantages. Nevertheless, it would be of interest and importance to perform similar quantification studies with ^{43}Sc in the future.

The empirical results reported herein should be considered in the light of some limitations. The export and analysis of raw data on the Biograph was not able due to restriction of the manufacturer. Moreover, the energy windows on both scanners were specified by the manufacturer and could not be scaled. Measurements with more than 80 MBq ^{44}Sc could not be performed due to limited production of ^{44}Sc by ^{44}Ti/^{44}Sc generator and time need for transport between the PET centers. Only one preclinical and one clinical scanner could be included. To obtain more comprehensive data, a multicenter study including several different PET systems is recommended. Furthermore, only one phantom for each system was used, thus variations of the object size were not contemplated. Further phantom measurements are needed in which also phantoms of different geometries are used to analyze the distribution of singles, randoms, scattered and corresponding noise-equivalent-counts.

7. Conclusion

Due to prompt gamma emission of ^{44}Sc, activity recovery is underestimated on PET systems calibrated for ^{18}F. However, clinical PET imaging of ^{44}Sc with acceptable quantitative accuracy appears feasible by using a single, constant correction factor.

Availability of data and materials

The datasets used and analyzed during the current study are available from the corresponding author on reasonable request.

Ethics approval and consent to participate

Not applicable.

Consent for publication

Not applicable.

Authors statement

All authors have read and consented to the final version of the manuscript.

Funding

Nothing to disclose.

CRediT authorship contribution statement

Florian Rosar: Study design, Data acquisition, Formal analysis, Writing - original draft. **Hendrik Bohnenberger:** Data acquisition, Writing - original draft. **Euy Sung Moon:** Chemical processing. **Frank Rösch:** Chemical processing. **Achim Denig:** Study design, Writing - review & editing. **Daniel Vincenz-Zörner:** Formal analysis. **Manuela A. Hoffmann:** Data acquisition. **Fadi Khreish:** Data acquisition. **Samer Ezziddin:** Writing - review & editing. **Mathias Schreckenberger:** Writing - review & editing. **Hans-Georg Buchholz:** Study design, Data acquisition, Formal analysis, Writing - original draft. **Andrea Schaefer-Schuler:** Study design, Data acquisition, Formal analysis, Writing - original draft.

Declaration of competing interest

The authors declare that they have no known competing financial interests or personal relationships that could have appeared to influence the work reported in this paper.

Acknowledgements

Not applicable.

List of abbreviations

Biograph	Siemens Biograph 40 mCT
CT	computer tomography
DOTA	1,4,7,10-tetraazacyclododecane-1,4,7,10-tetraacetic acid
EANM	European Association of Nuclear Medicine
EARL	ResEARch 4 Life
FOV	field of view
LSO	lutetium oxyorthosilicate
LYSO	lutetium-yttrium oxyorthosilicate
MRI	magnetic resonance imaging
nanoScan	Mediso nanoScan PET/MRI
NEMA	National Electrical Manufactures Association
OSEM	ordered subset expectation maximization
PET	positron emission tomography
PGC	prompt gamma correction
PMMA	polymethylmethacrylate
PSF	point-spread function
PSMA	prostate specific membrane antigen
TLC	thin-layer chromatography
TOF	time-of-flight
VOI	volume of interest

Appendix A. Supplementary data

Supplementary data to this article can be found online at https://doi.org/10.1016/j.apradiso.2021.109599.

References

Boellaard, R., Delgado-Bolton, R., Oyen, W.J.G., Giammarile, F., Tatsch, K., Eschner, W., Verzijlbergen, F.J., Barrington, S.F., Pike, L.C., Weber, W.A., Stroobants, S., Delbeke, D., Donohoe, K.J., Holbrook, S., Graham, M.M., Testanera, G., Hoekstra, O. S., Zijlstra, J., Visser, E., Hoekstra, C.J., Pruim, J., Willemsen, A., Arends, B., Kotzerke, J., Bockisch, A., Beyer, T., Chiti, A., Krause, B.J., 2015. FDG PET/CT: EANM procedure guidelines for tumour imaging: version 2.0. Eur. J. Nucl. Med. Mol. Imag. 42, 328–354. https://doi.org/10.1007/s00259-014-2961-x.

Braad, P.E.N., Hansen, S.B., Thisgaard, H., Høilund-Carlsen, P.F., 2015. PET imaging with the non-pure positron emitters: ^{55}Co, ^{86}Y and ^{124}I. Phys. Med. Biol. 60, 3479–3497. https://doi.org/10.1088/0031-9155/60/9/3479.

Buchholz, H.G., Herzog, H., Förster, G.J., Reber, H., Nickel, O., Rösch, F., Bartenstein, P., 2003. PET imaging with yttrium-86: comparison of phantom measurements acquired with different PET scanners before and after applying background subtraction. Eur. J. Nucl. Med. Mol. Imag. 30, 716–720. https://doi.org/10.1007/s00259-002-1112-y.

Bunka, M., Müller, C., Vermeulen, C., Haller, S., Türler, A., Schibli, R., van der Meulen, N.P., 2016. Imaging quality of ^{44}Sc in comparison with five other PET radionuclides using Derenzo phantoms and preclinical PET. Appl. Radiat. Isot. 110, 129–133. https://doi.org/10.1016/j.apradiso.2016.01.006.

Cal-González, J., Lage, E., Herranz, E., Vicente, E., Udias, J.M., Moore, S.C., Park, M.-A., Dave, S.R., Parot, V., Herraiz, J.L., 2015. Simulation of triple coincidences in PET. Phys. Med. Biol. 60, 117–136. https://doi.org/10.1088/0031-9155/60/1/117.

Conti, M., Eriksson, L., 2016. Physics of pure and non-pure positron emitters for PET: a review and a discussion. EJNMMI Phys 3, 8. https://doi.org/10.1186/s40658-016-0144-5.

Domnanich, K.A., Eichler, R., Müller, C., Jordi, S., Yakusheva, V., Braccini, S., Behe, M., Schibli, R., Türler, A., van der Meulen, N.P., 2017. Production and separation of ^{43}Sc for radiopharmaceutical purposes. EJNMMI Radiopharm Chem 2, 14. https://doi.org/10.1186/s41181-017-0033-9.

Domnanich, K.A., Müller, C., Farkas, R., Schmid, R.M., Ponsard, B., Schibli, R., Türler, A., van der Meulen, N.P., 2016. ^{44}Sc for labeling of DOTA- and NODAGA-functionalized peptides: preclinical in vitro and in vivo investigations. EJNMMI Radiopharm Chem 1, 8. https://doi.org/10.1186/s41181-016-0013-5.

Eigner, S., Vera, D.R.B., Fellner, M., Loktionova, N.S., Piel, M., Lebeda, O., Rösch, F., Roß, T.L., Henke, K.E., 2013. Imaging of protein synthesis: in vitro and in vivo evaluation of ^{44}Sc-DOTA-Puromycin. Mol. Imag. Biol. 15, 79–86. https://doi.org/10.1007/s11307-012-0561-3.

Eppard, E., de la Fuente, A., Benešová, M., Khawar, A., Bundschuh, R.A., Gärtner, F.C., Kreppel, B., Kopka, K., Essler, M., Rösch, F., 2017. Clinical translation and first in-human use of [^{44}Sc]Sc-PSMA-617 for PET imaging of metastasized castrate-resistant prostate cancer. Theranostics 7, 4359–4369. https://doi.org/10.7150/thno.20586.

Filosofov, D.V., Loktionova, N.S., Rösch, F., 2010. A ^{44}Ti/^{44}Sc radionuclide generator for potential application of ^{44}Sc-based PET-radiopharmaceuticals. Radiochim. Acta 98, 149–156. https://doi.org/10.1524/ract.2010.1701.

Herzog, H., Tellmann, L., Scholten, B., Coenen, H.H., Qaim, S.M., 2008. PET imaging problems with the non-standard positron emitters Yttrium-86 and Iodine-124. Q. J. Nucl. Med. Mol. Imaging 52, 159–165.

Honarvar, H., Müller, C., Cohrs, S., Haller, S., Westerlund, K., Karlström, A.E., van der Meulen, N.P., Schibli, R., Tolmachev, V., 2017. Evaluation of the first ^{44}Sc-labeled Affibody molecule for imaging of HER2-expressing tumors. Nucl. Med. Biol. 45, 15–21. https://doi.org/10.1016/j.nucmedbio.2016.10.004.

Huclier-Markai, S., Alliot, C., Kerdjoudj, R., Mougin-Degraef, M., Chouin, N., Haddad, F., 2018. Promising scandium radionuclides for nuclear medicine: a review on the production and Chemistry up to in vivo proofs of concept. Cancer Biother. Radiopharm. 33, 316–329. https://doi.org/10.1089/cbr.2018.2485.

Huclier-Markai, S., Sabatie, A., Ribet, S., Kubícek, V., Paris, M., Vidaud, C., Hermann, P., Cutler, C.S., 2011. Chemical and biological evaluation of scandium(III)-polyaminopolycarboxylate complexes as potential PET agents and radiopharmaceuticals. Radiochim. Acta 99, 653–662. https://doi.org/10.1524/ract.2011.1869.

Kaalep, A., Burggraaff, C.N., Pieplenbosch, S., Verwer, E.E., Sera, T., Zijlstra, J., Hoekstra, O.S., Oprea-Lager, D.E., Boellaard, R., 2019. Quantitative implications of the updated EARL 2019 PET–CT performance standards. EJNMMI Phys 6, 28. https://doi.org/10.1186/s40658-019-0257-8.

Kaalep, A., Sera, T., Rijnsdorp, S., Yaqub, M., Talsma, A., Lodge, M.A., Boellaard, R., 2018. Feasibility of state of the art PET/CT systems performance harmonisation. Eur. J. Nucl. Med. Mol. Imag. 45, 1344–1361. https://doi.org/10.1007/s00259-018-3977-4.

Khawar, A., Eppard, E., Sinnes, J., Roesch, F., Ahmadzadehfar, H., Kürpig, S., Meisenheimer, M., Gaertner, F., Essler, M., Bundschuh, R., 2018. [^{44}Sc]Sc-PSMA-617 biodistribution and dosimetry in patients with metastatic castration-resistant prostate carcinoma. Clin. Nucl. Med. 43, 323–330. https://doi.org/10.1097/RLU.0000000000002003.

Koumarianou, E., Loktionova, N.S., Fellner, M., Roesch, F., Thews, O., Pawlak, D., Archimandritis, S.C., Mikolajczak, R., 2012. ^{44}Sc-DOTA-BN[2-14]NH_2 in comparison to ^{68}Ga-DOTA-BN[2-14]NH_2 in pre-clinical investigation. Is ^{44}Sc a potential radionuclide for PET? Appl. Radiat. Isot. 70, 2669–2676. https://doi.org/10.1016/j.apradiso.2012.08.004.

Krajewski, S., Cydzik, I., Abbas, K., Bulgheroni, A., Simonelli, F., Holzwarth, U., Bilewicz, A., 2013. Cyclotron production of ^{44}Sc for clinical application. Radiochim. Acta 101, 333–338. https://doi.org/10.1524/ract.2013.2032.

Kull, T., Ruckgaber, J., Weller, R., Reske, S., Glatting, G., 2004. Quantitative imaging of yttrium-86 pet with the ecat exact Hr^+ in 2D mode. Cancer Biother. Radiopharm. 19, 482–490. https://doi.org/10.1089/cbr.2004.19.482.

Lima, T.V.M., Gnesin, S., Nitzsche, E., Ortega, P.G., Müller, C., van der Meulen, N.P., 2020. First phantom-based quantitative assessment of scandium-44 using a commercial PET device. Front. Physiol. 8, 241. https://doi.org/10.3389/fphy.2020.00241.

Lubberink, M., Herzog, H., 2011. Quantitative imaging of ^{124}I and ^{86}Y with PET. Eur. J. Nucl. Med. Mol. Imag. 38, 10–18. https://doi.org/10.1007/s00259-011-1768-2.

Majkowska-Pilip, A., Bilewicz, A., 2011. Macrocyclic complexes of scandium radionuclides as precursors for diagnostic and therapeutic radiopharmaceuticals. J. Inorg. Biochem. 105, 313–320. https://doi.org/10.1016/j.jinorgbio.2010.11.003.

Mikolajczak, R., van der Meulen, N.P., Lapi, S.E., 2019. Radiometals for imaging and theranostics, current production, and future perspectives. J. Label. Compd. Radiopharm. 62, 615–634. https://doi.org/10.1002/jlcr.3770.

Müller, C., Domnanich, K.A., Umbricht, C.A., van der Meulen, N.P., 2018. Scandium and terbium radionuclides for radiotheranostics: current state of development towards clinical application. Br. J. Radiol. 91, 20180074. https://doi.org/10.1259/bjr.20180074.

Nagy, G., Dénes, N., Kis, A., Szabó, J.P., Berényi, E., Garai, I., Bai, P., Hajdu, I., Szikra, D., Trencsényi, G., 2017. Preclinical evaluation of melanocortin-1 receptor (MC1-R) specific ^{68}Ga- and ^{44}Sc-labeled DOTA-NAPamide in melanoma imaging. Eur. J. Pharmaceut. Sci. 106, 336–344. https://doi.org/10.1016/j.ejps.2017.06.026.

National Electrical Menufacturers Association (NEMA), 2008. Performance Measurements of Small Animal Positron Emission Tomographs. NEMA Standards Publication NU, 4-2008.

Pruszyński, M., Loktionova, N.S., Filosofov, D.V., Rösch, F., 2010. Post-elution processing of ^{44}Ti/^{44}Sc generator-derived ^{44}Sc for clinical application. Appl. Radiat. Isot. 68, 1636–1641. https://doi.org/10.1016/j.apradiso.2010.04.003.

Pruszyński, M., Majkowska-Pilip, A., Loktionova, N.S., Eppard, E., Roesch, F., 2012. Radiolabeling of DOTATOC with the long-lived positron emitter ^{44}Sc. Appl. Radiat. Isot. 70, 974–979. https://doi.org/10.1016/j.apradiso.2012.03.005.

Roesch, F., 2012. Scandium-44: benefits of a long-lived PET radionuclide available from the ^{44}Ti/^{44}Sc generator system. Curr. Rad. 5, 187–201. https://doi.org/10.2174/1874471011205030187.

Rosar, F., Buchholz, H.-G., Michels, S., Hoffmann, M.A., Piel, M., Waldmann, C.M., Rösch, F., Reuss, S., Schreckenberger, M., 2020. Image quality analysis of ^{44}Sc on two preclinical PET scanners: a comparison to 68Ga. EJNMMI Phys 7, 16. https://doi.org/10.1186/s40658-020-0286-3.

Rösch, F., Herzog, H., Qaim, S., 2017. The beginning and development of the theranostic approach in nuclear medicine, as exemplified by the radionuclide pair ^{86}Y and ^{90}Y. Pharmaceuticals 10, 56. https://doi.org/10.3390/ph10020056.

Severin, G.W., Engle, J.W., Valdovinos, H.F., Barnhart, T.E., Nickles, R.J., 2012. Cyclotron produced ^{44g}Sc from natural calcium. Appl. Radiat. Isot. 70, 1526–1530. https://doi.org/10.1016/j.apradiso.2012.04.030.

Singh, A., van der Meulen, N.P., Müller, C., Klette, I., Kulkarni, H.R., Türler, A., Schibli, R., Baum, R.P., 2017. First-in-Human PET/CT imaging of metastatic neuroendocrine neoplasms with cyclotron-produced ^{44}Sc-DOTATOC: a proof-of-concept study. Cancer Biother. Radiopharm. 32, 124–132. https://doi.org/10.1089/cbr.2016.2173.

Umbricht, C.A., Benešová, M., Schmid, R.M., Türler, A., Schibli, R., van der Meulen, N.P., Müller, C., 2017. ^{44}Sc-PSMA-617 for radiotheragnostics in tandem with ^{177}Lu-PSMA-617—preclinical investigations in comparison with ^{68}Ga-PSMA-11 and ^{68}Ga-PSMA-617. EJNMMI Res. 7, 9. https://doi.org/10.1186/s13550-017-0257-4.

van der Meulen, N.P., Bunka, M., Domnanich, K.A., Müller, C., Haller, S., Vermeulen, C., Türler, A., Schibli, R., 2015. Cyclotron production of ^{44}Sc: from bench to bedside. Nucl. Med. Biol. 42, 745–751. https://doi.org/10.1016/j.nucmedbio.2015.05.005.

Walczak, R., Krajewski, S., Szkliniarz, K., Sitarz, M., Abbas, K., Choiński, J., Jakubowski, A., Jastrzębski, J., Majkowska, A., Simonelli, F., Stolarz, A., Trzcińska, A., Zipper, W., Bilewicz, A., 2015. Cyclotron production of ^{43}Sc for PET imaging. EJNMMI Phys 2. https://doi.org/10.1186/s40658-015-0136-x.